AIAA Paper 97-1774

Advances in Numerical Boundary Conditions for Computational Aeroacoustics†

Christopher K.W. Tam*
Florida State University
Tallahassee, FL 32306-3027

Abstract

Advances in Computational Aeroacoustics (CAA) depend critically on the availability of accurate, nondispersive, least dissipative computation algorithm as well as high quality numerical boundary treatments. This paper focuses on the recent developments of numerical boundary conditions. In a typical CAA problem, one often encounters two types of boundaries. Because a finite computation domain is used, there are external boundaries. On the external boundaries, boundary conditions simulating the solution outside the computation domain are to be imposed. Inside the computation domain, there may be internal boundaries. On these internal boundaries, boundary conditions simulating the presence of an object or surface with specific acoustic characteristics are to be applied. Numerical boundary conditions, both external or internal, developed for simple model problems are reviewed and examined. Numerical boundary conditions for real aeroacoustic problems are also discussed through specific examples. The paper concludes with a description of some much needed research in numerical boundary conditions for CAA.

1. Introduction

A physical problem is defined mathematically by the governing equations and boundary conditions. When the governing equations are discretized to be solved computationally, the resulting finite difference equations are usually of higher order than the original partial differential equations. This is because high order schemes are needed to minimize numerical dispersion, an important requirement of Computational Aeroacoustics (CAA). The use of high order schemes will be assumed throughout this paper. High order finite difference equations support extraneous solutions that are not solutions of the partial differential equations. Thus to ensure a quality solution, a set of numerical boundary conditions must be specified such that not only the physical boundary conditions are faithfully reproduced but also the amplitude of the extraneous solutions, if generated, would be minimized.

A computation domain is inevitably finite in size. The result is that part of the physical domain is lost in the numerical simulation. It is, therefore, important that whatever takes place in the lost domain should have very little influence on the solution inside the computation domain. If this is not the case, the effects must be simulated by the boundary conditions imposed on the boundaries of the computation domain. For exterior aeroacoustics problems, a set of nonreflecting or outflow boundary conditions are needed at the external boundaries. The purpose of the nonreflecting or outflow boundary conditions is to allow the radiated sound waves and the convected vorticity and entropy waves to leave the computation domain smoothly without reflection.

The main objective of this paper is to provide an assessment of the recent advances in the formulation of numerical boundary conditions for aeroacoustics problems. In CAA, numerical boundary conditions are often developed for idealized model problems. In practical applications, they must be modified or extended to account for the presence of a nonuniform and sometimes unknown mean flow. In many cases, the outgoing wave amplitude is not necessarily small. So linear boundary conditions would need to be adjusted to allow the exit of nonlinear waves. Issues of this kind will also be examinined and discussed in this paper.

Broadly speaking, CAA boundary conditions can be classified into six categories. They are:

1. Radiation boundary conditions.
2. Outflow boundary conditions.
3. Wall boundary conditions.
4. Impedance boundary conditions.
5. Radiation/outflow boundary conditions with incoming acoustics or vorticity waves.
6. Radiation boundary conditions for ducted environments.

The first three categories of boundary conditions are also needed in standard Computational Fluid Dynamics (CFD). However, owing to the presence of acoustic and vorticity waves, the actual boundary conditions used in CAA are very different from those

* Distinguished Research Professor, Department of Mathematics. Associate Fellow AIAA.

used in traditional CFD. The last three categories of boundary conditions appear to be unique to CAA problems.

The need for the above types of boundary conditions is best illustrated by considering the two computational aeroacoustics problems shown in figures 1 and 2. Figure 1 shows the computation domain for numerical simulation of jet noise generation. The jet flow leaves the computation domain along boundary AB. Here the imposition of a set of outflow boundary conditions to allow the jet flow, sound, vorticity and entropy waves to exit smoothly would be most appropriate. Along boundary $BCDE$, radiation boundary conditions are required. Along the nozzle wall, wall boundary conditions are necessary. Figure 2 shows the computation domain for numerical simulation of fan noise radiation from a jet engine inlet. An important component of fan noise is generated by the interaction of the ingested vorticity waves and the rotor inside the engine. To suppress fan noise, a standard practice is to install sound absorbing liners on the inner surface of the engine inlet as shown in figure 2. These liners are represented mathematically by an impedance boundary condition. Along the exterior boundary $CDEF$, radiation boundary conditions with incoming vorticity waves are needed for the numerical simulation. Along internal boundary AB, radiation boundary conditions for ducted environment are required to simulate the internal propagation of acoustic duct modes inside the jet engine.

The rest of this paper is as follows. In Section 2, numerical boundary conditions developed using idealized flow models will be examined and compared. In Section 3, boundary conditions developed for more realistic aeroacoustics problems are presented. These two sections form the main part of this paper. Section 4 concludes with a discussion of the challenges and future directions of development in numerical boundary conditions for CAA.

2. Boundary Conditions Based on Idealized Model Problems

Most numerical boundary conditions available in the literature were developed for idealized model problems. Idealization, in some cases, are necessary to make it possible for a rigorous derivation of the boundary conditions. From the point of view that boundary conditions are local relations, the use of local approximations to formulate first-order boundary conditions is quite justified. The development of numerical boundary conditions for the acoustic wave equation has continued for many years. A recent review was given by Givoli[1]. For numerical boundary conditions relevant to CAA for which the Euler or Navier-Stokes equations are used, brief reviews can be found in the articles by Tam[2] and Lele[3].

2.1 Radiation/Inflow and Outflow Boundary Conditions

It is well known that in a uniform mean flow the linearized Euler equations support three types of disturbances. They are the acoustic waves, the vorticity waves and the entropy waves. The acoustic waves propagate at sound speed relative to the mean flow. The vorticity as well as the entropy waves are frozen patterns convected downstream by the mean flow. Because of the presence of the three types of wave disturbances, each having distinct propagation characteristics, the outgoing disturbances present at the inflow and outflow boundaries are very different. At an inflow boundary, the only outgoing disturbances are acoustic waves. At an outflow boundary, in addition to the acoustic waves, both vorticity and entropy waves are convected out by the mean flow. Due to this distinctive difference, some authors choose to separate radiation/inflow boundary conditions and outflow boundary conditions as two different types of boundary conditions. Here we will do so whenever clarity demands.

There have been many proposed radiation/inflow and outflow boundary conditions based on totally different considerations. For convenience, we will group them into five types as follows.

(a) Characteristics Based Boundary Conditions

Thompson[4,5] and Poinsat & Lele[6] proposed to treat the problem as one-dimensional near the boundary of the computation domain. The coordinate in the direction normal to the boundary is taken as the spatial coordinate. For Euler equations in one dimension, a full set of characteristics can be easily found. Thompson, Poinsat & Lele used these characteristics to form boundary conditions involving only outgoing waves. However, in two- or three-dimensional problems, there are no true characteristics. The characteristics boundary conditions work well for acoustic disturbances incident nearly normally on the boundary. They do not give good results at grazing angle of incidence or when there is a strong mean flow tangential to the boundary.

(b) Boundary Conditions Derived from Asymptotic Solutions

Bayliss & Turkel[7,8], Hagstrom & Hariharan[9]

and Tam & Webb[10] derived radiation and outflow boundary conditions by means of the asymptotic solutions of the governing equations. In the case of small amplitude disturbances superimposed on a uniform mean flow of density ρ_0, pressure p_0 and velocity u_0 in the x-direction, the linearized Euler equations in two dimensions are,

$$\frac{\partial \mathbf{U}}{\partial t} + \frac{\partial \mathbf{E}}{\partial x} + \frac{\partial \mathbf{F}}{\partial y} = \mathbf{H} \tag{1}$$

where

$$\mathbf{U} = \begin{bmatrix} \rho \\ u \\ v \\ p \end{bmatrix}, \quad \mathbf{E} = \begin{bmatrix} \rho_0 u + \rho u_0 \\ u_0 u + \frac{p}{\rho_0} \\ u_0 v \\ u_0 p + \gamma p_0 u \end{bmatrix}, \quad \mathbf{F} = \begin{bmatrix} \rho_0 v \\ 0 \\ \frac{p}{\rho_0} \\ \gamma p_0 v \end{bmatrix}.$$

The nonhomogeneous term $\mathbf{H}$ on the right side of (1) represents distributed unsteady sources. By using Fourier-Laplace transforms, Tam & Webb[10] showed that the initial value problem of (1) has asymptotic solutions consisting of acoustic, vorticity and entropy waves. These asymptotic solutions have the form

(i) Acoustic waves

$$\begin{bmatrix} \rho \\ u \\ v \\ p \end{bmatrix} \sim \frac{F(\frac{r}{V(\theta)} - t, \theta)}{r^{\frac{1}{2}}} \begin{bmatrix} \frac{1}{a_0^2} \\ \widehat{u}(\theta) \\ \widehat{v}(\theta) \\ 1 \end{bmatrix} + O\left(r^{-\frac{3}{2}}\right) \tag{2}$$

where (r, θ) are the polar coordinates. $V(\theta) = u_0 \cos\theta + a_0(1 - M^2 \sin^2\theta)^{\frac{1}{2}}$, $M = \frac{u_0}{a_0}$, $a_0 = (\frac{\gamma p_0}{\rho_0})^{\frac{1}{2}}$ is the speed of sound.

(ii) Vorticity waves

$\rho = p = 0$

$$\begin{bmatrix} u \\ v \end{bmatrix} = \begin{bmatrix} \frac{\partial \Psi}{\partial y} \\ -\frac{\partial \Psi}{\partial y} \end{bmatrix} \tag{3}$$

where

$$\Psi = \begin{cases} \Psi(x - u_0 t, y), & x \to +\infty \\ 0, & x \to -\infty \end{cases}$$

(iii) Entropy waves

$u = v = p = 0$

$$\rho = \begin{cases} \chi(x - u_0 t, y), & x \to +\infty \\ 0, & x \to -\infty \end{cases} \tag{4}$$

In (2) to (4), the functions F, Ψ and χ depend on the initial condition and the unsteady source distribution.

At boundaries where there are only outgoing acoustic waves, a set of radiation boundary conditions can be derived by eliminating the unknown function F from (2) by first taking the t (time) and r derivatives. The resulting radiation boundary conditions are,

$$\left(\frac{1}{V(\theta)}\frac{\partial}{\partial t} + \frac{\partial}{\partial r} + \frac{1}{2r}\right) \begin{bmatrix} \rho \\ u \\ v \\ p \end{bmatrix} = 0 + O\left(r^{-\frac{5}{2}}\right). \tag{5}$$

At the outflow region, the outgoing disturbances consist of a combination of acoustic, vorticity and entropy waves, that is, a direct sum of (2), (3) and (4). It turns out, it is possible to eliminate the unknown functions F, Ψ and χ, and upon using the linearized momentum equations of (1), to obtain the following set of outflow boundary conditions.

$$\begin{aligned} &\frac{\partial \rho}{\partial t} + u_0 \frac{\partial \rho}{\partial x} = \frac{1}{a_0^2}\left(\frac{\partial p}{\partial t} + u_o \frac{\partial p}{\partial x}\right) \\ &\frac{\partial u}{\partial t} + u_0 \frac{\partial u}{\partial x} = -\frac{1}{\rho_0}\frac{\partial p}{\partial x} \\ &\frac{\partial v}{\partial t} + u_o \frac{\partial v}{\partial x} = -\frac{1}{\rho_0}\frac{\partial p}{\partial y} \\ &\frac{1}{V(\theta)}\frac{\partial p}{\partial t} + \cos\theta \frac{\partial p}{\partial x} + \sin\theta \frac{\partial p}{\partial y} + \frac{p}{2r} = 0. \end{aligned} \tag{6}$$

Extensive numerical experiments testing the accuracy of (5) and (6) have been carried out. The results indicate that radiation boundary conditions (5) and outflow boundary conditions (6) are extremely effective, provided the sources are sufficiently far from the boundary of the computation domain. When there are sources located close to the boundary, the quality of the numerical solution is somewhat degraded.

(c) Absorbing Boundary Conditions

A different idea to deal with exterior boundary conditions is to use an absorbing layer. An absorbing layer usually consists of 10 to 20 mesh points in which damping terms are introduced to damp out the incident waves. The development of absorbing boundary conditions has been pursued by many investigators including Engquist & Majda[11], Higdon[12,13], Kosloff & Kosloff[14] and Jiang & Wong[15].

In a more recent work, the idea of absorbing the incident wave was extended and refined by Colonius *et*

al. into a sponge and exit zone with grid stretching and filtering. Their work is directly related to the earlier work by Rai & Moin[17]. Similar proposal but without grid stretching was advanced before by Israeli and Orszag[18]. A somewhat different approach was suggested by Ta'asan & Nark[19]. They artificially modified the governing equations in a buffer zone so that the mean flow becomes supersonic in the outward direction. This idea was further extended by Hayden and Turkel[20] to the full Euler equations in conservation form. Most recently Freund[21] proposed a zonal approach combining the absorbing boundary idea and the technique of Ta'asan & Nark.

(d) Perfectly Matched Layer

In an absorbing layer, the addition of artificial damping terms to the governing equations for the purpose of damping out the incidence disturbances also can lead to substantial reflections at the interface. Berenger[22,23], in his work on computational electromagnetics, found that it is possible to formulate an absorbing layer without reflection. Such a layer has come to be known as a perfectly matched layer (PML). It has found applications in computational aeroacoustics, elastic wave propagation[24] and other areas. Hu[25] was the first to apply PML to acoustics problems governed by the linearized Euler equations with uniform mean flow. He has since extended his work to nonuniform flow and for the fully nonlinear Euler equations[26]. Further applications of PML can be found in the recent works of Hu and coworkers[27,28]. One great advantage of the PML method is that if the mean flow is uniform the boundary of the computation domain can be put very close to the acoustic sources. This sometimes allows the use of a small computation domain.

Although PML has been demonstrated to perform exceedingly well computationally yet the PML equations with a mean flow are unstable. Consider the computation of small amplitude disturbances superimposed on a uniform mean flow in a computation domain as shown in figure 3. Let's use $\Delta x = \Delta y$ (the mesh size) as the length scale, a_0 (the sound speed) as the velocity scale, $\frac{\Delta x}{a_0}$ as the time scale, $\rho_0 a_0^2$ (where ρ_0 is the mean density) as the pressure scale. The dimensionless governing equations in the PML are formed by splitting the linearized Euler equations according to the spatial derivatives. An absorption term is added to each of the equations with spatial derivative in the direction normal to the layer. For example, for the PML on the right boundary of figure 3, region (1), the governing equations are[25],

$$\begin{aligned}
&\frac{\partial u_1}{\partial t} + \sigma u_1 + M_x \frac{\partial}{\partial x}(u_1 + u_2) + \frac{\partial}{\partial x}(p_1 + p_2) = 0 \\
&\frac{\partial u_2}{\partial t} + M_y \frac{\partial}{\partial y}(u_1 + u_2) = 0 \\
&\frac{\partial v_1}{\partial t} + \sigma v_1 + M_x \frac{\partial}{\partial x}(v_1 + v_2) = 0 \\
&\frac{\partial v_2}{\partial t} + M_y \frac{\partial}{\partial y}(v_1 + v_2) + \frac{\partial}{\partial y}(p_1 + p_2) = 0 \\
&\frac{\partial p_1}{\partial t} + \sigma p_1 + M_x \frac{\partial}{\partial x}(p_1 + p_2) + \frac{\partial}{\partial x}(u_1 + u_2) = 0 \\
&\frac{\partial p_2}{\partial t} + M_y \frac{\partial}{\partial y}(p_1 + p_2) + \frac{\partial}{\partial y}(v_1 + v_2) = 0
\end{aligned} \tag{7}$$

where M_x and M_y are the mean flow Mach numbers in the x and y directions. σ is the absorption coefficients.

Suppose we look for solutions with (x, y, t) dependence in the form $\exp[i(\alpha x + \beta y - \omega t)]$. It is easy to find from (7) that the dispersion relations of the PML region are,

$$\left(1 - \frac{\alpha M_x}{\omega + i\sigma} - \frac{\beta M_y}{\omega}\right)^2 - \frac{\alpha^2}{(\omega + i\sigma)^2} - \frac{\beta^2}{\omega^2} = 0 \tag{8}$$

$$1 - \frac{\alpha M_x}{\omega + i\sigma} - \frac{\beta M_y}{\omega} = 0 \tag{9}$$

In the limit $\sigma \to 0$, (8) and (9) become the dispersion relations of the acoustic and the vorticity waves of the linearized Euler equations. (8) is a quadric equation in ω. It has two extra roots in addition to the two modified acoustic modes. For small σ, the two spurious roots are damped but one of the modified acoustic roots is unstable. For larger σ, numerical solutions indicate that one of the spurious roots becomes unstable. In any case, the equation splitting procedure and the addition of an absorption term, both are vital to the suppression of reflections at the interface between the computation domain and the PML, inadvertently lead to instabilities.

For small σ, the roots of (8) and (9) can be found by perturbation. Let,

$$\omega^{(a)} = \omega_0^{(a)} + \sigma\omega_1^{(a)} + \sigma^2\omega_2^{(a)} + \dots \tag{10}$$

$$\omega^{(v)} = \omega_0^{(v)} + \sigma\omega_1^{(v)} + \sigma^2\omega_2^{(v)} + \dots \tag{11}$$

where the roots of (8) and (9) are designated by a superscript 'a' (for acoustic waves) and 'v' (for

vorticity waves). Substitution of (10) and (11) into (8) and (9), it is straightforward to find,

$$\omega_0^{(a)} = \omega_+, \quad \omega_-, \quad 0, \quad 0 \tag{12}$$

where

$$\omega_\pm = (\alpha M_x + \beta M_y) \pm (\alpha^2 + \beta^2)^{\frac{1}{2}}$$

$$\omega_1^{(a)} = i \left[\frac{-\omega_\pm^2 + (\alpha M_x + \beta M_y)\omega_\pm + (1-M^2)\beta^2 - \alpha\beta M_x M_y}{\omega_\pm(\omega_\pm - \alpha M_x - \beta M_y)} \right] \tag{13}$$

$$\omega_0^{(v)} = \alpha M_x + \beta M_y, \quad 0 \tag{14}$$

$$\omega_1^{(v)} = \frac{-i}{1 + (\frac{M_y}{M_x})(\frac{\beta}{\alpha})} \tag{15}$$

Clearly if $\omega_1^{(a)}$ or $\omega_1^{(v)}$ has positive imaginary part, the mode is unstable. (13) has a simple interpretation in the case $M_y = 0$. In this special case, (13) reduces to

$$\omega_1^{(a)} = i \left[\frac{\alpha^2 M_x^2 - \alpha\omega_\pm M_x}{\beta^2 + \alpha\omega_\pm M_x - \alpha^2 M_x^2} \right]. \tag{16}$$

For acoustic waves with negative phase velocity; i.e., $\alpha\omega_\pm < 0$ (the group velocity can, however, be positive) the numerator of (16) is positive, there will be values of β^2 for which $\omega_1^{(a)}$ is purely positive imaginary. Similarly, from (15), for $\frac{\beta}{\alpha} < 0$ and $|\frac{\beta}{\alpha}| > \frac{M_x}{M_y}$, $\omega_1^{(v)}$ is also purely positive imaginary. Thus the PML equations in the presence of a uniform flow with $M_x \neq 0$ support unstable solutions.

In a finite difference computation the dimensionless wavenumbers α and β are restricted to the range of $-\pi$ to π. Following the work of Hu[25], we will assume a PML of width equal to 10 mesh spacings. For a mean flow of $M_x = 0.3$, a value of $\sigma = 1.5$ would be quite sufficient to reduce the intensity of the incident acoustic waves by a factor of 10^5. Figure 4 shows a contour map of the growth rate of the most unstable wave ($\mathrm{Im}(\omega)$ is largest) in the $\alpha - \beta$ plane for such a mean flow. The maximum growth rate is 0.035. In carrying out numerical simulation over a long period of time, even a weak instability could be a source of trouble. It is, therefore, desirable to suppress the instability. One way to suppress the instability and, at the same time, retain perfectly matched condition at the edge of the computation domain is to add artificial selective damping terms[29] to the discretized form of (7). The design of the artificial selective damping stencil is such that there is almost no damping on the long (physical) waves. Thus the inclusion of these terms in the finite difference scheme should not alter the perfectly matched condition for the physical waves. With artificial damping included, the discretized form of the first equation of (7) according to the 7-point stencil Dispersion-Relation-Preserving (DRP) scheme[10] is (Note: all the other equations are to be treated in a similar way),

$$K_{\ell,m}^{(n)} = -\sigma u_{1\ell,m}^{(n)} - M_x \sum_{j=-3}^{3} a_j [u_{1\ell+j,m}^{(n)} + u_{2\ell+j,m}^{(n)} + p_{1\ell+j,m}^{(n)} + p_{2\ell+j,m}^{(n)}] - \frac{1}{R_\Delta} \left[\sum_{j=-3}^{3} d_j \left(u_{1\ell+j,m}^{(n)} + u_{1\ell,m+j}^{(n)} \right) \right] \tag{17}$$

$$u_{1\ell,m}^{(n+1)} = u_{1\ell,m}^{(n)} + \Delta t \sum_{j=0}^{3} b_j K_{\ell,m}^{(n-j)} \tag{18}$$

where R_Δ is the artificial mesh Reynolds numbers. By applying Fourier transform analysis to (17) and (18) following Ref. [29], the damping rate introduced by the last term of (17) is

$$D(\alpha,\beta) = \frac{1}{R_\Delta} \sum_{j=-3}^{3} d_j \left(e^{-ij\alpha} + e^{-ij\beta} \right) \tag{19}$$

Figure 5 shows the contours of constant damping rate for $R_\Delta = 1.0$. The coefficient d_j's are those corresponding to $\sigma = 0.3\pi$ given in the appendix of Ref. [2]. Figure 6 shows the combined growth and damping rate of figures 4 and 5 for $R_\Delta = 0.46$. As can be seen, the instability is completely suppressed. Note that for a PML with a width of 10 mesh spacings, waves with a wavenumber α smaller than $\frac{2\pi}{10}$ cannot be excited. This band of wavenumbers lies within the two vertical dotted lines of figure 6.

(e) Other Methods

In addition to the above four types of methods, nonreflecting boundary conditions have also been developed by a number of investigators using special methodology. This includes the works of Giles[30], Atkins & Casper[31], Colonius[32], Scott *et al.*[33], Kroner[34] and Roe[35]. Giles used a Fourier series approach. His work appears to have been motivated by turbomachinery noise and flow consideration.

(f) Evaluation of Radiation/Inflow and Outflow Boundary Conditions

During the last few years, there have been a number of papers reporting the results of evaluations of the performance and accuracy of a number of proposed radiation and outflow boundary conditions. Hixson *et al.*[36] employed a CAA problem with known exact solution to evaluate the quasi-one-dimensional characteristic boundary conditions of Thompson[4,5], the Fourier series boundary conditions of Giles and the asymptotic boundary conditions of Tam & Webb[10] and Bayliss & Turkel[7,8]. They reported that the Tam & Webb boundary conditions gave satisfactory results whereas the Thompson's boundary conditions produced significant reflections.

Hayden & Turkel[37] reported their experience in using the boundary condition of a number of investigators[4,5,7,8,9,10,33,34,35]. However, the various proposed boundary conditions were not implemented in the computation in an identical manner. A definitive comparison becomes impossible. Dong[38], in a study of radiation boundary conditions for nonuniform mean flow, performed a direct comparison of the results using his method and those of the Thompson's and Tam & Webb's boundary conditions. The numerical results confirm the finding of Hixson *et al.*[36], namely, the quasi-one-dimensional characteristics boundary conditions can cause significant reflections and inaccuracies.

It is also worthwhile to mention that two CAA workshops on benchmark problems have been held since 1994. Some of the benchmark problems were designed to test radiation/inflow and outflow boundary conditions. In each of the workshop proceedings[39,40], there is a section on comparisons of computed results and exact (nearly exact) solutions. They provide a measure of the quality of the various numerical boundary conditions used.

2.2 Wall Boundary Conditions for High-Order Schemes

In CAA, high order finite difference schemes are used because they have less numerical dispersion. However, a high order finite difference equation support spurious solutions that have no relationship to the original partial differential equation. These spurious solutions are unavoidably excited at a wall. For aeroacoustics problems, the spurious waves are of two types, propagating waves with short wave lengths and spatially damped waves. Thus when an acoustic wave pulse impinges on a wall, in addition to the reflected waves, spurious short waves will also be emitted in a high order finite difference solution. Furthermore, the spatially damped waves would also be generated. But they decay as they propagate away from the wall. Effectively they form a numerical boundary layer on the wall surface.

There are two major difficulties in developing wall boundary conditions for high order finite difference schemes. First, high order finite difference equations require additional boundary conditions, beyond the physical boundary conditions of the original problem, to define a unique solution. These additional boundary conditions, or the way to handle the need for these boundary conditions, must be found so that only very small amplitude spurious waves are excited. Second, in the discretized system, each flow variable at either an interior or boundary mesh point is governed by an algebraic equation (discretized form of the partial differential equation). The number of unknowns is exactly equal to the number of equations. Thus there will be too many equations and not enough unknowns if it is insisted that the boundary conditions at the wall mesh point are satisfied also. This is, perhaps, one of the major differences between partial differential equations and finite difference equations.

In the literature, there is an absence of suggestions as how to impose wall boundary condition for high order schemes except for the work of Tam & Dong[41]. They proposed to use backward difference stencils as a wall is approached. This eliminates the need for extra boundary conditions. To provide enough unknowns to enforce the physical wall boundary conditions as well as to allow the discretized governing equations to be satisfied at mesh points on the wall, they suggested including ghost values at ghost points. Ghost points are mesh points immediately outside the computation domain. The number of ghost values to be included is equal to the number of physical wall boundary conditions per enforcement point. Tam & Dong carried out an analysis of the problem of reflection of plane acoustic waves by a plane wall using the ghost point method. They found that the intensity of the reflected spurious short waves is largest for normal incidence but is less than 0.4% of the amplitude of the incident wave if a resolution of 10 mesh spacings per acoustic wavelength is used. The thickness of the numerical boundary layer (defined as the distance from the wall at which the spurious damped numerical wave solution drops to 0.1% of the magnitude of the incident wave) is a little over one mesh spacing. The ghost point method has since been extended by Kurbatskii & Tam[42] for applications to curved wall surfaces us-

ing Cartesian mesh. Numerical results obtained in a number of test cases agreed well with exact solutions.

For acoustic wave scattering problems, Chung & Morris[43] proposed an Impedance Mismatched Method (IMM). In this method, solid bodies are replaced by a new fluid medium with a large characteristic impedance, ρa. When the characteristic impedance of the new fluid medium is infinite, it can be shown that the incident waves are completely reflected. The advantage of the IMM method is that the entire computation domain including the scattering bodies can be regarded as a continuous fluid region making the programming exceedingly simple. However, unlike the ghost point method, the IMM cannot be used for viscous problems.

2.3 Impedance Boundary Condition

One of the most successful methods for suppressing fan noise radiating out the inlets of jet engines is to install acoustic liners inside the front part of the engine inlet as shown in figure 2. Mathematically, a liner is represented by an impedance boundary condition. The impedance, Z, is a complex quantity. If the time dependence is taken to be $e^{-i\omega t}$ then Z is related to the two real parameters of the liner R, the resistance, and X, the reactance, by

$$Z = R - iX.$$

Ref. [44] provides a good introduction and many references to the impedance of liners. In the past, impedance boundary condition was analyzed in the frequency domain. For time marching computation, an equivalent time-domain impedance boundary condition is required.

Presently, two entirely different approaches for developing time-domain impedance boundary condition are available. Both approaches have limitations. Ozyoruk & Long[45,46], following the works of Sullivan[47] and Penny[48] in computational electromagnetics, employed the z-transform method in implementing the impedance boundary conditions in the time-domain. This method provides more flexibility in fitting the frequency dependence of the resistance and reactance of the liner to experimental measurements. Tam & Auriault[49] used a differential formulation of time-domain impedance boundary condition. Both methods are constrained by spurious numerical instability. For treatment of broadband noise problems, the formulation of Tam & Auriault is restricted by numerical instability to a 3 parameter model. Further improvements on these methods are obviously desirable.

2.4 Radiation and Outflow Boundary Conditions with Incoming Acoustic and Vorticity Waves

As depicted in figure 2, there are aeroacoustics problems for which unsteady incoming acoustic or vorticity waves are an important part of the problem. For this class of problems, the boundary conditions must allow the incoming disturbances to propagate in and the outgoing disturbances to leave the computation domain smoothly. There are two ways to treat these boundary requirements. We will refer to them as the nonhomogeneous boundary conditions method and the split variable method.

The nonhomogeneous boundary conditions approach recognizes that the computed variables are the direct sum of the incoming and outgoing disturbances. Thus on using subscripts 'in' and 'out' to denote the part of the flow variables associated with the incoming and outgoing disturbances, the outgoing disturbances can be expressed as the difference between the computed variables and the prescribed incoming disturbances; e.g.,

$$\rho_{\text{out}} = \rho - \rho_{\text{in}}. \tag{20}$$

Now at the inflow boundary, the outgoing acoustic waves satisfy the radiation boundary condition (5). Therefore, by substitution of (20) and similar expressions into (5), a set of nonhomogeneous radiation boundary conditions is obtained,

$$\left[\frac{1}{V(\theta)}\frac{\partial}{\partial r} + \frac{\partial}{\partial t} + \frac{1}{2r}\right]\begin{bmatrix}\rho\\ u\\ v\\ p\end{bmatrix} = \left[\frac{1}{V(\theta)}\frac{\partial}{\partial r} + \frac{\partial}{\partial t} + \frac{1}{2r}\right]\begin{bmatrix}\rho_{\text{in}}\\ u_{\text{in}}\\ v_{\text{in}}\\ p_{\text{in}}\end{bmatrix}. \tag{21}$$

In (21) the nonhomogeneous terms on the right side represent the known incoming waves. In Ref. [42], the plane acoustic wave scattering problem was calculated numerically using (21) as the boundary conditions. It has been found that if the computation is to be carried out with low spatial resolution, then an improvement in the numerical accuracy is obtained if the exact finite difference solution of the incoming disturbances is used on the right side of (21). At an outflow boundary, nonhomogeneous outflow boundary conditions similar to (21) may be derived from (6).

Another way to generate the incoming waves is to divide the computation domain into an interior and a boundary region. In the interior region, the computed variables are the sum of the outgoing and incoming disturbances. In the boundary region (3 mesh points for the 7-point DRP scheme), the governing equations are either the boundary conditions derived from asymptotic solutions of Section 2.1(b) or the absorbing boundary conditions of Section 2.1(c) or the PML equations of Section 2.1(d). The computed variables are the outgoing disturbances only. Whenever a derivative stencil extends to the other region, the value of the variable required can be obtained by using (20) and similar equations. Here the inflow variables are given so either ρ or ρ_{out}, whichever is appropriate can be easily found. In this way, the incoming disturbances are generated at the stencil overlapping part (overlapping with the boundary region) of the interior region.

2.5 Radiation Boundary Conditions for Ducted Environment

For the fan noise radiation problem illustrated in figure 2, when the sound waves, generated by the cutting of the ingested vorticity waves by the rotor, reach the opening of the jet engine inlet, part of them are reflected back. The reflected waves would be propagating in the form of duct modes if the internal area of the engine inlet varies slowly. Unlike acoustic waves in the free field, duct modes are dispersive. They are formed by the continuous reflection of sound waves by the walls of the duct. Their propagation characteristics are very different from acoustic waves in free space. As a result, not all the radiation and outflow boundary conditions discussed in Section 2.1 are applicable along boundary AB of figure 2.

In the Second CAA Workshop on Benchmark Problems[40], several benchmark problems require the use of radiation boundary conditions in a ducted environment for their solutions. For single frequency time periodic problems, Tam *et al.*[50] developed a set of such radiation boundary conditions using the duct modes as the basis. Hu and Manthey[28], on the other hand, used the PML and variable splitting method to form such radiation boundary conditions. It is necessary to point out that in a ducted environment, the dispersion relation of the PML equations are not the same as those given in (8) and (9). They are related to the duct modes. To ensure numerical stability, artificial selective damping is again required in the PML. The value of the artificial mesh Reynolds number, R_Δ, necessary to ensure stability can be found in much the same way as in Section 2.1(d).

3. Boundary Conditions for Real Problems

The numerical boundary conditions discussed in the above section are based largely on simplified models. Real problems, however, are generally more complex. In many of these problems, numerical boundary conditions do not simply play a single role such as letting the outgoing disturbances exit smoothly with minimal reflections. They are to perform multiple tasks. In most problems that are of technological significance, the mean flow is nonuniform. Further, because of computer memory constraint and run time limitation, the size of the computation domain is usually smaller than ideal. The small computer domain, forcing the boundary to be closer to the source or objects in the flow, puts additional demand on the design of high quality numerical boundary conditions. There does not appear to have a systematic way of classifying numerical boundary conditions for real problems. We will illustrate, by specific examples, below how some of the model boundary conditions can be modified and extended for applications in practical CAA problems of current interest.

3.1 Radiation Boundary Conditions for Simulating Jet Noise Generation

Let us return to the computation domain for simulating jet noise generation in figure 1. For practical reasons, the size of the computation domain is typically 30 to 40 diameters in the axial direction and 20 to 30 diameters in the radial direction. These dimensions are smaller than those of the anechoic chambers in most physical experiments. Because of the proximity of the computation boundary to the jet flow, the boundary conditions along boundary $BCDE$ are burdened with multiple tasks. Obviously, the boundary conditions must be transparent to the outgoing acoustic waves radiated from the jet. In addition, the boundary conditions must impose the ambient conditions on the numerical solution. In other words, they specify the static conditions far away from the jet. Furthermore, the jet entrains a large volume of ambient fluid. The entrainment flow velocity at the computation boundary is although small yet not entirely negligible. For high quality numerical simulation, the boundary conditions must, therefore, allow the entrainment flow to enter the computation domain smoothly as well.

In a recent work, Tam & Dong[51] considered the need to formulate a set of radiation as well as out-

flow boundary conditions for situations where the mean flow was nonuniform. They provided a generalization of the asymptotic radiation boundary conditions (5) and outflow boundary conditions (6). Let $\overline{\rho}$, $\overline{u}$, $\overline{v}$ and $\overline{p}$ be the weakly nonuniform mean flow at the boundary of the computation domain, an appropriate set of radiation boundary conditions, in 3 dimensions, was found to be,

$$\frac{1}{V(\theta,r)}\frac{\partial}{\partial t}\begin{bmatrix}\rho\\u\\v\\p\end{bmatrix} + \left[\sin\theta\frac{\partial}{\partial r}+\cos\theta\frac{\partial}{\partial x}+\frac{1}{(r^2+x^2)^{\frac{1}{2}}}\right]\begin{bmatrix}\rho-\overline{\rho}\\u-\overline{u}\\v-\overline{v}\\p-\overline{p}\end{bmatrix}=0 \tag{22}$$

where (r,ϕ,x) are the cylindrical coordinates, θ is the polar angle (in spherical coordinates) with the x-axis as the polar axis. (u,v) are the velocity components in the axial (x) and radial (r) directions. $V(\theta,r)=\overline{u}\cos\theta+\overline{v}\sin\theta+[\overline{a}^2-(\overline{v}\cos\theta-\overline{u}\sin\theta)^2]^{\frac{1}{2}}$ and $\overline{a}$ is the speed of sound.

In their work on numerical simulation of the generation of axisymmetric screech tones from imperfectly expanded supersonic jets (see Ref. [52] for a description of the jet screech phenomenon) Tam & Shen[53] considered a computation domain nearly identical to that of figure 1. They used (22) as the basis to develop the necessary radiation-entrainment flow numerical boundary conditions. It was recognized that the entrainment flow at the boundary of the computation domain would be influenced by the jet flow outside the computation domain. To develop an asymptotic entrainment flow solution Tam & Shen divided the jet into many evenly spaced segments as shown in figure 7. The jet extended beyond the computation domain to 60 diameters downstream. The mass fluxes across the boundaries of each segment was found using empirical jet flow data. The difference of the mass fluxes at the two ends of each segment of the jet gave the amount of entrainment flow for the particular segment. This entrainment was then simulated by a point source located at the center of the segment. The asymptotic solution for a point sink located on the x-axis at x_s in a compressible fluid is given by (a subscript 'e' is used to indicate entrainment flow),

$$\begin{aligned}
\frac{\rho_e}{\rho_\infty} &= 1-\frac{Q^2}{32\pi^2[(x-x_s)^2+r^2]^2}+\cdots\\
\frac{u_e}{a_\infty} &= -\frac{Q(x-x_s)}{4\pi[(x-x_s)^2+r^2]^{\frac{3}{2}}}+\cdots\\
\frac{v_e}{a_\infty} &= -\frac{Qr}{4\pi[(x-x_s)^2+r^2]^{\frac{3}{2}}}+\cdots\\
\frac{p_e}{\rho_\infty a_\infty^2} &= \frac{1}{\gamma}-\frac{Q^2}{32\pi^2[(x-x_s)^2+r^2]^2}+\cdots
\end{aligned} \tag{23}$$

where ρ_∞, a_∞ and γ are the ambient gas density, sound speed and the ratio of specific heats. Q, the strength of the sink, has dimensions of $\rho_\infty a_\infty D^2$; D is the jet diameter. On replacing $(\overline{\rho},\overline{u},\overline{v},\overline{p})$ of (22) by (ρ_e,u_e,v_e,p_e) of (23) and by summing over the contributions from all the sinks, the desired radiation entrainment flow boundary conditions are obtained.

Figure 8 shows the entrainment flow streamlines of a Mach 1.13 cold jet from a convergent nozzle obtained by numerical simulation. It is worthwhile to point out that along the right-hand boundary BC, the mean flow actually flows out of the computation domain, exactly as observed experimentally in the case of a free jet. This streamline pattern would be very different had the entrainment flow outside the computation domain not been included in the sink flow calculation. If a cut-off were imposed at the right boundary of the computation domain, a recirculation flow pattern would emerge. This, however, is inconsistent with experimental observation.

3.2 Outflow and Jet Axis Boundary Conditions for Simulating Jet Noise Generation

Jets are inherently unstable. The instability waves of jets play an important role in jet noise generation[52]. The instability waves, once excited at the nozzle lip region, grow rapidly as they propagate in the downstream direction. Since the jet spreads out in the downstream direction, it follows that the shear gradient and hence the instability growth rate decreases farther and farther downstream. Eventually the wave would reach a location downstream where it becomes damped. From this point on, the wave amplitude decreases continuously all the way to the outflow boundary. In the work of Tam & Shen[53] the outflow boundary was located at 30 jet diameters downstream. At this distance, the amplitudes of the decaying instability waves (sometimes

referred to as large turbulence structures when there is less coherence) are not small. To account for the weak nonlinearities of the outflow disturbances, it is possible to nonlinearize the outflow boundary conditions (6) by replacing the linearized terms by their nonlinear counterpart. This yields (in cylindrical coordinates),

$$\frac{\partial \rho}{\partial t} + u\frac{\partial \rho}{\partial x} = \frac{1}{a^2}\left(\frac{\partial p}{\partial t} + u\frac{\partial p}{\partial x}\right)$$

$$\frac{\partial u}{\partial t} + u\frac{\partial u}{\partial x} + v\frac{\partial u}{\partial r} = -\frac{1}{\rho}\frac{\partial p}{\partial x} \qquad (24)$$

$$\frac{\partial v}{\partial t} + u\frac{\partial v}{\partial x} + v\frac{\partial v}{\partial r} = -\frac{1}{\rho}\frac{\partial p}{\partial r}$$

$$\frac{1}{V(\theta)}\frac{\partial p}{\partial x} + \cos\theta\frac{\partial p}{\partial x} + \sin\theta\frac{\partial p}{\partial r} + \frac{p-\bar{p}}{(x^2+r^2)^{\frac{1}{2}}} = 0$$

where $\bar{p}$ is the static pressure calculated by the entrainment flow model at the edge of the jet flow at the outflow boundary. In their jet screech tones simulation work, Tam & Shen[53] reported that (24) provided very satisfactory numerical results. No reflection of any significance had been detected.

In cylindrical coordinates, the governing equations have an apparent singularity at the jet axis ($r \to 0$). For instance, the continuity equation may be written in the form,

$$\frac{\partial \rho}{\partial t} + \frac{\partial \rho v}{\partial r} + \frac{\partial \rho u}{\partial x} + \frac{1}{r}\frac{\partial \rho w}{\partial \phi} + \frac{\rho v}{r} = 0. \qquad (25)$$

To handle the apparent singularity, a jet axis boundary condition may be derived by taking the formal limit of (25) as $r \to 0$. On noting that as $r \to 0$, $v \to 0$ while $w \to 0$ faster than r, the formal limit of (25) is,

$$\frac{\partial \rho}{\partial t} + 2\frac{\partial \rho v}{\partial r} + \frac{\partial \rho u}{\partial x} = 0. \qquad (26)$$

(26), which has no apparent singularity at $r = 0$, is to be enforced at all the mesh points along the jet axis.

Experience indicates that the use of (26) at $r = 0$ inevitably leads to the generation of spurious short waves at the x-axis in a time marching simulation. The reason for this is simply that there is an abrupt change in the governing equations between the jet axis and the first row of mesh point off the axis. Such discontinuous change always leads to the radiation of short waves. For problems with axisymmetry, one may use the half-mesh displacement method[50] to avoid the discontinuity. The half mesh displacement method does not involve a change in governing equations. It depends on the extension of the computation domain to the region $r < 0$ by symmetry and antisymmetry arguments.

3.3 Numerical Simulation of Airframe Noise Generation

During landing with the wing flaps of an aircraft down, the unsteady flow over the airframe is an important source of noise. In a series of experimental investigation, Kendall & Ahtye[54] identified a number of airframe noise sources; referred to as the flap side-edge noise, gap noise and trailing edge noise. One possible gap noise generation mechanism is unsteady flow separation around the gap between the wing and the flap. This possibility was investigated using a 2-D numerical simulation by Thies, Tam & Reddy[55]. For simplicity, both the wing and flap were approximated by flat plates as shown in figure 9. This figure, from the numerical simulation, shows large unsteady separation on the suction side of the flap. In performing the numerical simulation, a relatively small computation domain was used. At a speed of Mach 0.15 and an angle of attack of 6 degrees, there is a steady loading on the wing-flap combination. The steady loading produces a distortion on the mean flow that extends all the way to the boundary of the computation domain. To achieve a reasonably accurate simulation, the numerical boundary conditions must not only allow the unsteady disturbances to leave the computation domain but also account for the mean flow distortion. Unlike the model problems of section 2 or the work of Ref. [51], the difficulty here in formulating a set of radiation boundary conditions is that the mean flow is unknown *a priori*.

In order to take into consideration the change in the mean flow at the boundary of the computation domain due to the presence of the wing-flap combination, one can first determine the forms of the asymptotic solutions of both the mean flow and the unsteady disturbances. This can be done by solving the linearized Euler equations. On using the wing chord L as the length scale, u_∞ (incoming velocity) as the velocity scale, $\frac{L}{u_\infty}$ as the time scale, ρ_∞ (the ambient gas density) as density scale and $\rho_\infty u_\infty^2$ as the pressure scale, the dimensionless linearized Euler equations are,

$$\frac{\partial \rho}{\partial t} + \cos\alpha\frac{\partial \rho}{\partial x} + \sin\alpha\frac{\partial \rho}{\partial y} + \left(\frac{\partial u}{\partial x} + \frac{\partial v}{\partial y}\right) = 0$$

$$\frac{\partial u}{\partial t} + \cos\alpha\frac{\partial u}{\partial x} + \sin\alpha\frac{\partial u}{\partial y} = -\frac{\partial p}{\partial x} \qquad (27)$$

$$\frac{\partial v}{\partial t} + \cos\alpha \frac{\partial v}{\partial x} + \sin\alpha \frac{\partial v}{\partial y} = -\frac{\partial p}{\partial y}$$

$$\frac{\partial p}{\partial t} + \cos\alpha \frac{\partial p}{\partial x} + \sin\alpha \frac{\partial p}{\partial y} + \frac{1}{M^2}\left(\frac{\partial u}{\partial x} + \frac{\partial v}{\partial y}\right) = 0$$

where M is the Mach number and α is the angle of attack. The time independent solution of (27) can be found by introducing a velocity potential $\Phi(x, y)$ defined by

$$u = \frac{\partial \Phi}{\partial x}, \quad v = \frac{\partial \Phi}{\partial y}$$
$$p = -\left(\cos\alpha \frac{\partial \Phi}{\partial x} + \sin\alpha \frac{\partial \Phi}{\partial y}\right), \quad \rho = M^2 p. \tag{28}$$

Substitution of (28) into (27) gives,

$$\left(\cos\alpha \frac{\partial}{\partial x} + \sin\alpha \frac{\partial}{\partial y}\right)\Phi$$
$$-\frac{1}{M^2}\left(\frac{\partial^2 \Phi}{\partial x^2} + \frac{\partial^2 \Phi}{\partial y^2}\right) = 0. \tag{29}$$

(29) can be manipulated into the Laplace equation by introducing a rotation and dilation of coordinates. The general solution of the Laplace equation can be expressed in the form of a Fourier series in polar coordinates. The lowest order nontrivial solution for large r is in the form of a logarithmic function. When rewritten in the Cartesian coordinates, it is found,

$$\Phi(x, y) \to A\,\ell n\Big[(x\cos\alpha + y\sin\alpha)^2$$
$$+ (1 - M^2)(x\sin\alpha - y\cos\alpha)^2\Big] \tag{30}$$

where A is an unknown constant. In the gap noise problem, A represents the as yet unknown loading on the wing-flap combination.

It is straightforward to find by substituting (30) into (28), after some algebra, the following asymptotic results.

$$\left(\frac{\partial}{\partial r} + \frac{1}{r}\right)\begin{bmatrix}\rho\\ u\\ v\\ p\end{bmatrix} = 0. \tag{31}$$

Since only the leading term is kept in (30), (31) is valid to order r^{-2} for large r. On the other hand, the asymptotic radiation boundary conditions for acoustic waves in a uniform mean flow, from (5), is

$$\left(\frac{1}{V(\theta)}\frac{\partial}{\partial t} + \frac{\partial}{\partial r}\right)\begin{bmatrix}\rho\\ u\\ v\\ p\end{bmatrix} = 0 + O\left(r^{-\frac{3}{2}}\right). \tag{32}$$

A combined asymptotic boundary conditions in 2 dimensions that reduces to (32) for the time dependent component and (31) for the time independent component is,

$$\left(\frac{1}{V(\theta)}\frac{\partial}{\partial t} + \frac{\partial}{\partial r} + \frac{1}{r}\right)\begin{bmatrix}\rho\\ u\\ v\\ p\end{bmatrix} = 0 + O\left(r^{-\frac{3}{2}}\right). \tag{33}$$

On following the same reasoning, it is easy to derive a corresponding set of outflow boundary conditions suitable for use in a relatively small computation domain where weakly nonuniform two-dimensional mean flow is present. The equations are,

$$\frac{\partial \rho}{\partial t} + \cos\alpha \frac{\partial \rho}{\partial x} + \sin\alpha \frac{\partial \rho}{\partial y}$$
$$= M^2\left(\frac{\partial p}{\partial t} + \cos\alpha \frac{\partial p}{\partial x} + \sin\alpha \frac{\partial p}{\partial y}\right)$$
$$\frac{\partial u}{\partial t} + \cos\alpha \frac{\partial u}{\partial x} + \sin\alpha \frac{\partial u}{\partial y} = -\frac{\partial p}{\partial x} \tag{34}$$
$$\frac{\partial v}{\partial t} + \cos\alpha \frac{\partial v}{\partial x} + \sin\alpha \frac{\partial v}{\partial y} = -\frac{\partial p}{\partial y}$$
$$\frac{1}{V(\theta)}\frac{\partial p}{\partial t} + \frac{\partial p}{\partial r} + \frac{p}{r} = 0.$$

Thies *et al.*[55] implemented (33) and (34) in their numerical simulations of gap noise and obtained very satisfactory results. Figure 10 shows the sound-pressure-level (SPL) contours in dB from the numerical simulation. The SPL contours below the wing form nearly concentric circles centered at the gap between the wing and the flap. This indicates that the source of noise originates from the gap region in agreement with the experimental observations of Kendall & Ahtye[54].

4. Concluding Remarks

During the last few years, a good deal of progress has been made in the development of numerical boundary conditions for CAA. Numerical examples have shown that many of these boundary conditions, when used in conjunction with high order finite difference schemes, are capable of providing high quality computational results. However, a closer scrutiny reveals that the predominant fraction of these recent works is devoted primarily to radiation and outflow boundary conditions. Other equally important types of boundary conditions such as wall boundary conditions, impedance boundary conditions do not appear to have received enough attention. The need for these other types of boundary conditions would definitely be greater in the future. For they are crucial to the application of CAA methods to fan noise, duct acoustics, propeller and turbomachinery noise problems.

In this paper, two very important items directly related to numerical boundary conditions have not been satisfactorily discussed. The first is the discretization and implementation of the numerical boundary conditions. Needless to say, the discretization process affects the accuracy and performance of a proposed boundary condition in a differential form. The implementation of the discretized boundary condition in relation to the time marching high order finite difference scheme used for the interior points would also have a significant impact on the overall accuracy and stability of the numerical solution. The second item is error estimate. From the point of view of designing a computational algorithm for the solution of a class of aeroacoustics problems, *a priori* estimate is essential. Here order of magnitude estimate is not very helpful. The real need is a quantitative error estimate. Most unfortunately, so far, very little work has been done. It is hoped that investigators interested in CAA would accept these two items as their immediate challenges.

Acknowledgment

The author wishes to thank Hao Shen, Laurent Auriault and Andrew Thies for their assistance. This work was supported by NASA Langley Research Center under Grant NAG 1-1776.

References

1. Givoli, D., "Non-Reflecting Boundary Conditions," Journal of Computational Physics, Vol. 94, May 1991, pp. 1–29.
2. Tam, C.K.W., "Computational Aeroacoustics: Issues and Methods," AIAA Journal, Vol. 33, Oct. 1995, pp. 1788–1796.
3. Lele, S.K., "Computational Aeroacoustics: A Review," AIAA Paper 97–0018, Jan. 1997.
4. Thompson, K.W., "Time Dependent Boundary Conditions for Hyperbolic Systems," Journal of Computational Physics, Vol. 68, Jan. 1987, pp. 1–24.
5. Thompson, K.W., "Time Dependent Boundary Conditions for Hyperbolic Systems, II," Journal of Computational Physics, Aug. Vol. 89, 1990, pp. 439–461.
6. Poinsot, T.J. and Lele, S.K., "Boundary Conditions for Direct Simulations of Compressible Viscous Flows," Journal of Computational Physics, Vol. 101, July 1992, pp. 104–129.
7. Bayliss, A. and Turkel, E., "Radiation Boundary Conditions for Wavelike Equations," Communications on Pure and Applied Mathematics, Vol. 33, Nov. 1980, pp. 707–725.
8. Bayliss, A. and Turkel, E., "Far Field Boundary Conditions for Compressible Flows," Journal of Computational Physics, Vol. 48, Nov. 1982, pp. 182–199.
9. Hagstrom, T. and Hariharan, S.I., "Accurate Boundary Conditions for Exterior Problems in Gas Dynamics," Mathematics of Computation, Vol. 51, Oct. 1988, pp. 581–597.
10. Tam, C.K.W. and Webb, J.C., "Dispersion-Relation-Preserving Finite Difference Schemes for Computational Acoustics," Journal of Computational Physics, Vol. 107, Aug. 1993, pp. 262–281.
11. Engquist, B. and Majda, A., "Absorbing Boundary Conditions for the Numerical Simulation of Waves," Mathematics of Computation, Vol. 31, July 1977, pp. 629–651.
12. Higdon, R.L., "Absorbing Boundary Conditions for Difference Approximations to the Multi-Dimensional Wave Equation," Mathematics of Computation, Vol. 47, Oct. 1986, pp. 629–651.
13. Higdon, R.L., "Numerical Absorbing Boundary Conditions for the Wave Equation," Mathematics of Computation, Vol. 49, July 1987, pp. 65–90.
14. Kosloff, R. and Kosloff, D., "Absorbing Boundaries for Wave Propagation Problems," Journal of Computational Physics, Vol. 63, April 1986, pp. 363–376.
15. Jiang, H. and Wong, Y.S., "Absorbing Boundary Conditions for Second Order Hyperbolic Equations," Journal of Computational Physics, Vol 88., May 1990, pp. 205–231.
16. Colonius, T., Lele, S.K., and Moin, P., "Boundary Conditions for Direct Computation of Aero-

dynamic Sound Generation," AIAA Journal, Vol. 31, Sept. 1993, pp. 1574–1582.

17. Rai, M.M., and Moin, P., "Direct Numerical Simulation of Transition and Turbulence in a Spatially Evolving Boundary Layer," Journal of Computational Physics, Vol. 109, 1993, pp. 169–192.
18. Israeli, M., and Orszag, S.A., "Approximation of Radiation Boundary Condition," Journal of Computational Physics, Vol. 41, 1981, pp. 115–135.
19. Ta'asan, S., and Nark, D.M., "An Absorbing Buffer Zone Technique for Acoustic Wave Propagation," AIAA Paper 95–0164, Jan. 1995.
20. Hayder, M.E., and Turkel, E., "On Buffer Layers as Non-Reflecting Computational Boundaries," AIAA paper 96–0273, Jan. 1996.
21. Freund, J.B., "Proposed Inflow/Outflow Boundary Condition for Direct Computation of Aerodynamic Sound," AIAA Journal, Vol. 35, April 1997, pp. 740-742.
22. Berenger, J.P., "A Perfectly Matched Layer for the Absorption of Electromagnetic Waves," Journal of Computational Physics, Vol. 114, 1994, pp. 182–200.
23. Berenger, J.P., "Three Dimensional Perfectly Matched Layer for the Absorption of Electromagnetic Waves," Journal of Computational Physics, Vol. 127, 1996, pp. 363-379.
24. Hastings, F.D., Schneider, J.B. and Broschat, S.L., "Application of the Perfectly Matched layer (PML) Absorbing Boundary Condition to Elastic Wave Propagation," Journal Acoustical Society America, Vol. 100, Nov. 1996, pp. 3061–3069.
25. Hu, F.Q., "On Absorbing Boundary Conditions for Linearized Euler Equations by a Perfectly Matched Layer," Journal of Computational Physics, Vol. 129, 1996, pp. 201–219.
26. Hu, F.Q., "On Perfectly Matched Layer As An Absorbing Boundary Condition," AIAA Paper 96–1664, May 1996.
27. Hayder, M., Hu, F.Q., and Hussaini, Y.M., "Toward Perfectly Absorbing Boundary Conditions for Euler Equations," AIAA Paper 97–2075, June 1997.
28. Hu, F.Q., and Manthey, J.L., "Application of PML Absorbing Boundary Conditions to the Benchmark Problems of Computational Aeroacoustics," in Proceedings of the Second Computational Aeroacoustics Workshop on Benchmark Problems, ed. C.K.W.Tam and J.C. Hardin, 1997 (to be published as a NASA CP).
29. Tam, C.K.W., Webb, J.C., and Dong, Z., "A Study of the Short Wave Components in Computational Acoustics," Journal of Computational Acoustics, Vol. 1, Mar. 1993, pp. 1–30.
30. Giles, M.B., "Nonreflecting Boundary Conditions for Euler Equation Calculations," AIAA Journal, Vol. 28, Dec. 1990, pp. 2050–2058.
31. Atkins, H., and Casper, J., "Nonreflective Boundary Conditions for High-Order Methods," AIAA Journal, Vol. 32, Mar. 1994, pp. 512–518.
32. Colonius, T., "Numerically Nonreflecting Boundary and Interface Conditions," AIAA Paper 96–1661, May 1996.
33. Scott, J.N., Mankbadi, R.R., Hayder, M.E. and Hariharan, S.I., "Outflow Boundary Conditions for the Computational Analysis of Jet Noise," AIAA Paper 93–4366, Oct. 1993.
34. Kroner, D., "Absorbing Boundary Conditions for the Linearized Euler Equations in 2-D," Mathematics of Computation, Vol. 57, 1991, pp. 153–167.
35. Roe, P., "Remote Boundary Conditions for Unsteady Multidimensional Aerodynamic Computations," Computers and Fluids Journal, Vol. 17, 1989, pp. 221–231.
36. Hixon, D.R., Shih, S., and Mankbadi, R.R., "Evaluation of Boundary Conditions for Computational Aeroacoustics," AIAA Journal, Vol. 33, Nov. 1995, pp. 2006–2012.
37. Hayder, M.E., and Turkel, E., "Nonreflecting Boundary Conditions for Jet Flow Computations," AIAA Journal, Vol. 33, Dec. 1995, pp. 2264–2270.
38. Dong, T.Z., "A Set of Simple Radiation Boundary Conditions for Acoustics Computations in Nonuniform Mean Flows," AIAA Paper 96–0274, Jan. 1996.
39. Hardin, J.C., Ristorcelli, J.R., and Tam, C.K.W., ICASE/LaRC workshop on Benchmark Problems in Computational Aeroacoustics. NASA CP 3300, May 1995.
40. Tam, C.K.W., and Hardin, J.C. Second Computational Aeroacoustics workshop on Benchmark Problems (to be published as a NASA CP, 1997).
41. Tam, C.K.W. and Dong, Z., "Wall Boundary Conditions for High-Order Finite Difference Schemes in Computational Aeroacoustics," Theoretical and Computational Fluid Dynamics, Vol. 8, 1994, pp. 303–322.
42. Kurbatskii, K.A., and Tam, C.K.W., "Cartesian Boundary Treatment of Curved Walls for High-

Order Computational Aeroacoustics Schemes," AIAA Journal, Vol. 35, Jan. 1997, pp. 133–140.

43. Chung, C., and Morris, P.J. "Acoustic Scattering from Two and Three-Dimensional Bodies," Proceedings of the First Joint CEAS/AIAA Aeroacoustics Conference, June 1995, Munich, Germany, pp. 55–63.
44. Motsinger, R.E., and Kraft, R.E., "Design and Performance of Duct Acoustic Treatment", in Aeroacoustics of Flight Vehicles: Theory and Practice, ed. H.H. Hubbard, NASA RP–1258, Aug. 1991, Chapter 14.
45. Ozyoruk, Y., and Long, L.L., "A Time-Domain Implementation of Surface Acoustic Impedance Condition With and Without Flow," AIAA Paper 96–1663, May 1996.
46. Ozyoruk, Y., and Long, L.L., "Impedance Boundary Conditions for Time-Domain Computational Aeroacoustics Methods", AIAA Paper 97–0021, Jan. 1997.
47. Sullivan, D.M., "Frequency-Dependent FDTD Methods Using z Transform," IEEE Transactions on Antennas and Propagation, Vol. 40, Oct. 1992, pp. 1223–1230.
48. Penny, C., "Scattering From Coated Targets Using a Frequency-Dependent Impedance Boundary Condition in the Finite Difference Time-Domain Method, "Ph.D. Thesis, The Pennsylvania State University, University Park, May 1995.
49. Tam, C.K.W., and Auriault, L., "Time-Domain Impedance Boundary Conditions for Computational Aeroacoustics," AIAA Journal, Vol. 34, May 1996, pp. 917–923.
50. Tam, C.K.W., Kurbatskii, K. and Fang, J., "Numerical Boundary Conditions for Computational Aeroacoustics Benchmark Problems", in Proceedings of the Second Computational Aeroacoustics Workshop on Benchmark Problems, ed. C.K.W. Tam and J.C. Hardin, 1997 (to be published as a NASA CP).
51. Tam, C.K.W. and Dong, Z., "Radiation and Outflow Boundary Conditions for Direct Computation of Acoustic and Flow Disturbances in a Nonuniform Mean Flow," Journal of Computational Acoustics, Vol. 4, 1996, pp. 175–201.
52. Tam, C.K.W., "Supersonic Jet Noise," Annual Review of Fluid Mechanics, Vol. 27, 1995, pp. 17–43.
53. Tam, C.K.W., and Shen, H., "Numerical Simulation of the Jet Screech Phenomenon Using Computational Aeroacoustics Method," First AFOSR International Conference on Direct Numerical Simulation and Large Eddy Simulation. (Abstract submitted) Aug., 1997, Ruston, Louisiana.
54. Kendall, J.M., and Ahtye, W.F., "Noise Generation by a Lifting Wing/Flop Combination at Reynolds Numbers to $2.8x10^6$," AIAA Paper 80–0035, Jan. 1980.
55. Thies, A.T., Tam, C.K.W., and Reddy, N.N., Airframe Noise via Numerical Simulation," to be published.

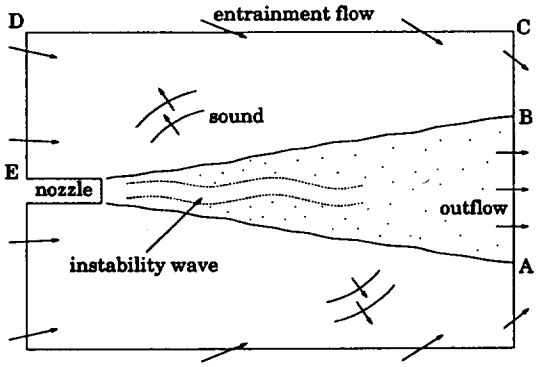

Figure 1. The computation domain for numerical simulation of jet noise generation

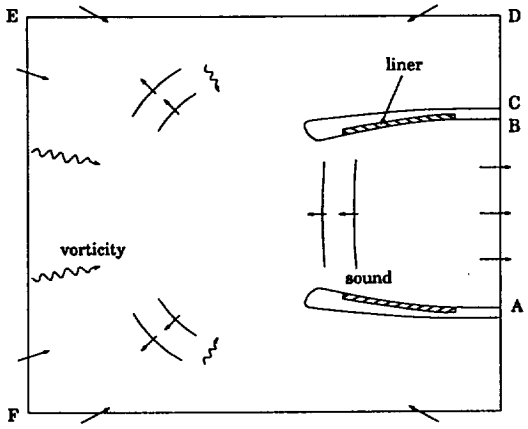

Figure 2. The computation domain for numerical simulation of fan noise radiation from a jet engin inlet

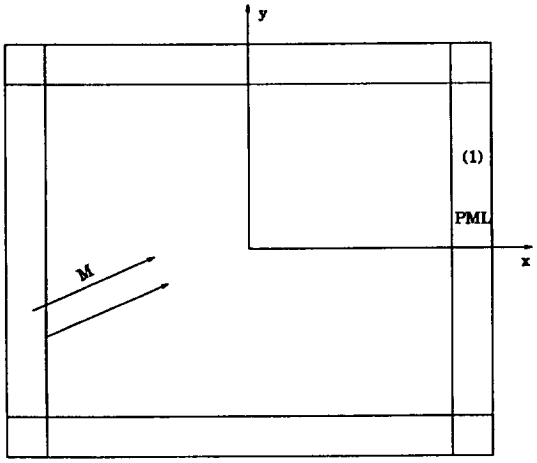

Figure 3. Two dimensional computation domain with Perfectly Matched Layers as boundaries

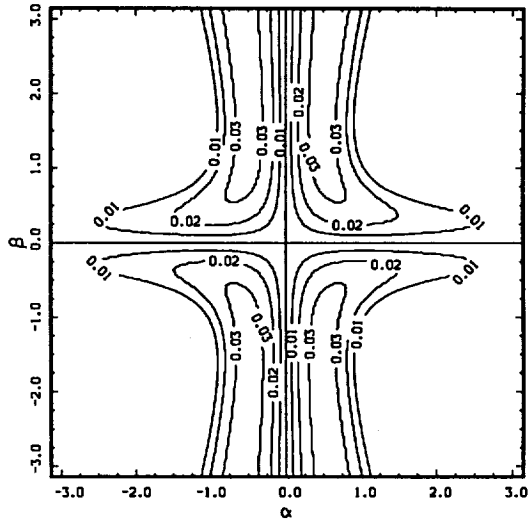

Figure 4. Contours of the growth rate of the most unstable wave in the $\alpha - \beta$ plane. $M_x = 0.3$, $M_y = 0$, $\sigma = 1.5$

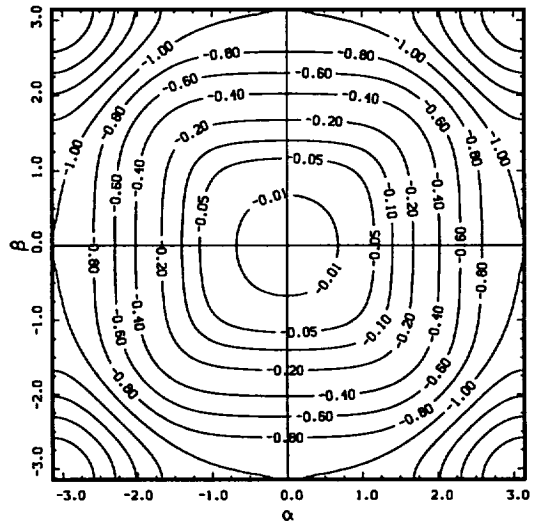

Figure 5. Contours of constant damping rate in the $\alpha - \beta$ plane.

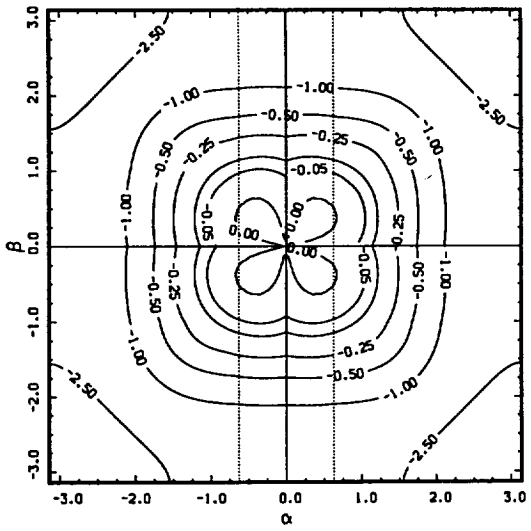

Figure 6. Contours of combined growth and damping rates for $R_\Delta = 0.46$

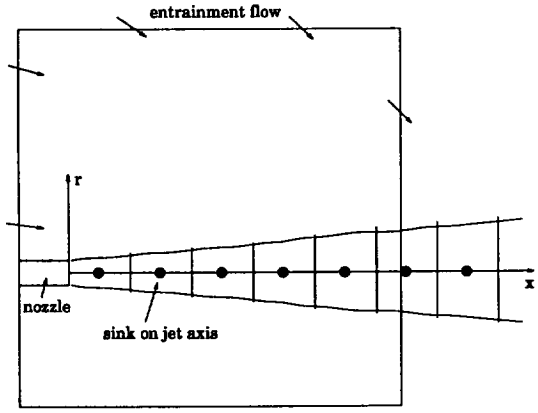

Figure 7. Determination of the entrainment flow of a supersonic jet by the point-sinks approximation

Figure 8. Computed streamlines of the entrainment flow around a supersonic screeching jet at $M = 1.13$

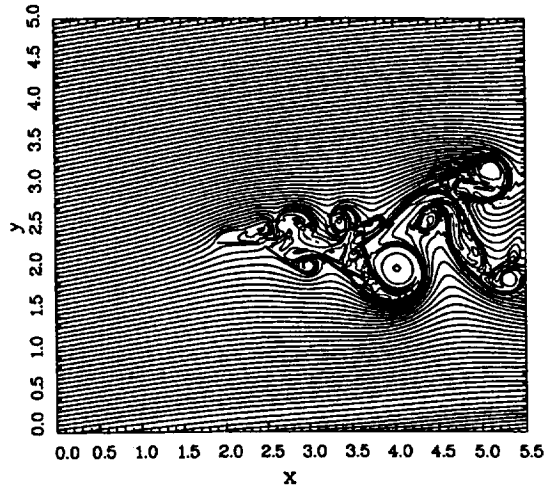

Figure 9. Streaklines of flow around a wing-flap combination at Mach 0.15 and 6 degrees angle of attack

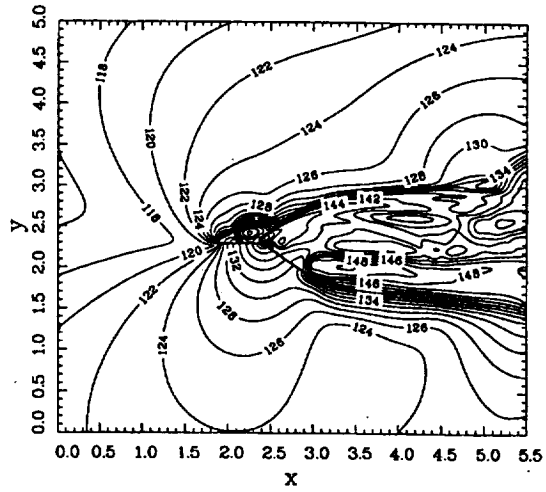

Figure 10. Sound-pressure-level contours obtained by numerical simulation of the flow around a wing-flap combination at Mach 0.15 and 6 degrees angle of attack